SURFACE PHYSICS
AND THIN FILMS

Structure and Electron Transport of Strontium Iridate Epitaxial Films

**Yu. V. Kislinskii[a, b], G. A. Ovsyannikov[a, c], A. M. Petrzhik[a], K. Y. Constantinian[a], *,
N. V. Andreev[d], and T. A. Sviridova[d]**

[a] *Kotel'nikov Institute of Radio Engineering and Electronics, Russian Academy of Sciences,
ul. Mokhovaya 11−7, Moscow, 125009 Russia*

[b] *Shubnikov Institute of Crystallography, Russian Academy of Sciences, Leninskii pr. 59, Moscow, 119333 Russia*

[c] *Chalmers University of Technology, Gothenburg, Sweden*

[d] *National University for Physics and Technology MISiS, Leninskii pr. 49, Moscow, 119991 Russia*

*e-mail: karen@hitech.cplire.ru

Received May 12, 2015

Abstract—The crystallographic and electrophysical properties of epitaxial $SrIrO_3$ films, in which the crystal lattice is deformed due to the mismatch between the lattice parameters of strontium iridate and the substrate, have been studied. Substrates (001) $SrTiO_3$, (001) $LaAlO_3$ + Sr_2AlTaO_6 (LSAT), (110) $NdGaO_3$, and (001) $LaAlO_3$ have been used. As a result of the deformation of the crystal lattice, the electrical resistivities of the films deposited on substrates with different lattice parameters differ by several times. The $SrIrO_3$ films with thickness $d = 90$ nm, grown on $SrTiO_3$ and LSAT substrates, have a nonmonotonic temperature dependence of the conductivity: type of the temperature dependence of the conductivity changes from metallic to dielectric at $T_L = 200−250$ K. The electrical resistance of the films with thicknesses less than 20 nm on all the substrates decreases exponentially with increasing temperature.

1. INTRODUCTION

In recent years, transition metal oxides with $5d$ orbitals have attracted considerable interest due to unique phase states formed because of the existence of strong spin−orbit and electron−electron interactions [1−3]. Such materials, among them iridates, were considered as paramagnetic metals with correlated states that are due to the existence of $5d$ states and a partially filled conduction band. Recently, it was theoretically shown that these materials can exhibit the properties of topological insulators, superconductors with an unusual superconducting state, systems with the quantum spin Hall effect, etc. [4−7]. Significant interest has been expressed by researchers in a series of iridates with the Ruddlesden−Popper structure $Sr_{n + 1}IrO_nO_{3n + 1}$ that consists of compounds with substantially different electronic states, from three-dimensional metal $SrIrO_3$ ($n = \infty$) to two-dimensional Mott insulator Sr_2IrO_4 ($n = 1$) with band splitting with $J_{eff} = 1/2$, and an insulator with a dielectric gap Sr_4IrO_6. Such iridates become insulators when the crystal field of the octahedron [8] splits degenerate states of $5d$ electrons into e_g and t_{2g} bands, and the partially filled t_{2g} band is split into the bands with $J_{eff} = 3/2$ and $1/2$ due to the strong spin−orbit interaction. In this case, the formation of the Mott gap induced by the

Coulomb interaction in the band with $J_{eff} = 1/2$ is energetically preferable. In the $SrIrO_3$ unit cell, six oxygen atoms are neighbors of an iridium atom, and only four oxygen atoms are neighbors of an iridium atom in the Sr_2IrO_4 unit cell. The decrease in the number of $5d$ orbitals of Ir decreases the band width and brings about the formation of a gap in the partially filled band with $J_{eff} = 1/2$ in Sr_2IrO_4. The gap of Ir $5d$ orbitals increases with the number of IrO_2 planes; as a result, perovskite $SrIrO_3$ becomes a metal with correlated electronic states [1].

The metal−insulator transition in $SrIrO_3$ was studied in [9−11]. Although it is known that the Ir−O bond length is almost unchanged, the angle of the Ir−O−Ir chain is prone to the influence of stresses in a $SrIrO_3$ film induced by a substrate [12, 13]. This can decrease the hopping-coupling energy between $5d$ orbitals and strongly influence the electron transport characteristics. This work presents the structural and transport studies of $SrIrO_3$ films grown on four single-crystal substrates, namely: (001) $SrTiO_3$, (001) $LaAlO_3$ + Sr_2AlTaO_6, (110) $NdGaO_3$, and (001) $LaAlO_3$, the crystal parameters of which determine the deformation of the film crystal lattice.

(a)

(110)SrIrO$_3$ (b)
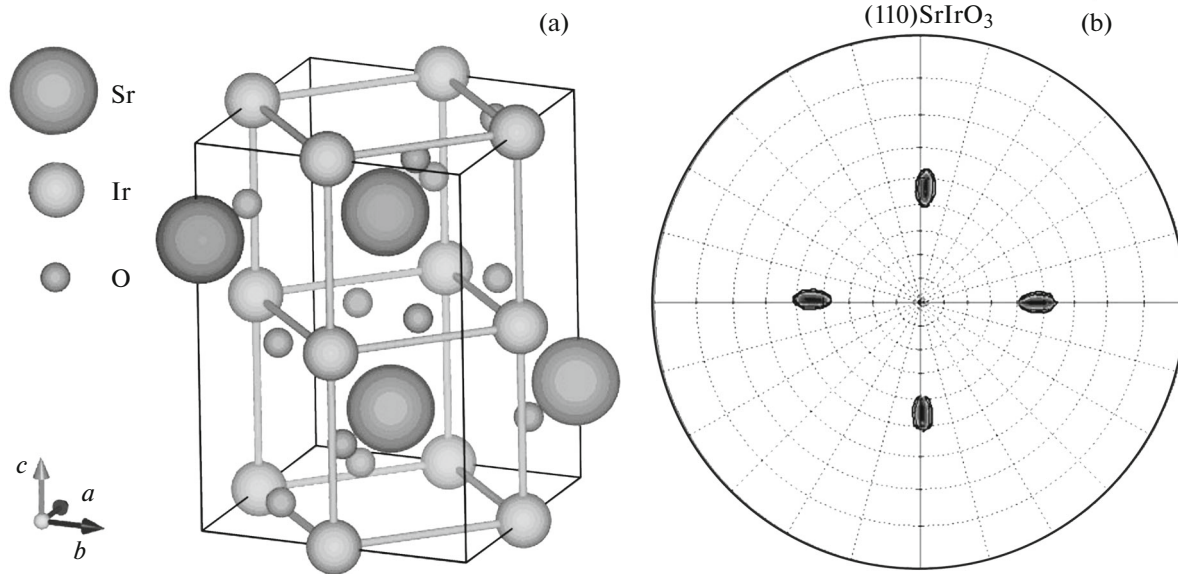
Fig. 1. (a) Schematic image of the orthorhombic phase of SrIrO$_3$ film. The orthorhombic unit cell has lattice parameters $a = 0.55617$ nm, $b = 0.55909$ nm, and $c = 0.78821$ nm. Using the simplified pseudocubic consideration of this phase, two unit cells can be represented as $a = b = c = 0.397$ nm. (b) Pole figure for the SrIrO$_3$/NdGaO$_3$ film measured at $2\theta = 31.9°$ for reflection (110) SrIrO$_3$.

2. EXPERIMENTAL SAMPLES

Among Sr$_{n+1}$Ir$_n$O$_{3n+1}$ iridates, we choose SrIrO$_3$ ($n = \infty$), the electronic properties of which are close to the properties of a three-dimensional metal. The stable modification of the SrIrO$_3$ compound (SIO) has a monoclinic structure (space group $C2/c$) with lattice parameters $a = 0.5604$ nm, $b = 0.9618$ nm, $c = 1.4170$ nm, and angle $\beta = 93.26°$); the structure can be represented as a monoclinic distortion of hexagonal structure of the $6H$-BaTiO$_3$ type [8, 14, 15]. Under high external pressure, the orthorhombic structure of SIO can form with lattice parameters $a = 0.55617$ nm, $b = 0.55909$ nm, and $c = 0.78821$ nm in the *Pbnm* symmetry [14, 15]; this structure can be considered as a pseudocube with lattice parameter $a = 0.398$ nm [11, 16]. A metastable orthorhombic structure of SIO can also form upon epitaxial growth of the film on a perovskite-like substrate [11, 16–18].

Epitaxial SIO films 10–90 nm in thickness were produced by laser ablation on single-crystal substrates of (001) SrTiO$_3$ (STO), (001) LaAlO$_3$ + Sr$_2$AlTaO$_6$ (LSAT), (110) NdGaO$_3$ (NGO), and (001) LaAlO$_3$ (LAO) at a temperature of 770°C and an oxygen pressure of 0.3 mbar. In the pseudocubic representation, the STO, LSAT, NGO, and LAO substrates have the crystal lattice parameters 0.390, 0.388, 0.386, and 0.378 nm, respectively.

The film structure on the (110) NGO substrate can be described as a perovskite with the lattice periods $a_f = b_f = c_f = 0.397$ nm (Fig. 1a). The existence of the pseudocubic crystal lattice (Fig. 1 shows two unit cells limited by iridium atoms) was determined by the mea-

surement of direct pole figures at various angles 2θ. Figure 1b shows the pole figure measured at $2\theta = 31.9°$ for reflections from the (110) SIO grown on an NGO substrate. Four (110) SIO peaks were detected at angles $\phi = 0°$, $90°$, $180°$, and $270°$ at angle $\psi = 45°$. It is seen that the arrangement of the peaks corresponds to the standard gnomostereographic projection of the cubic lattice with the center for plane (001), which
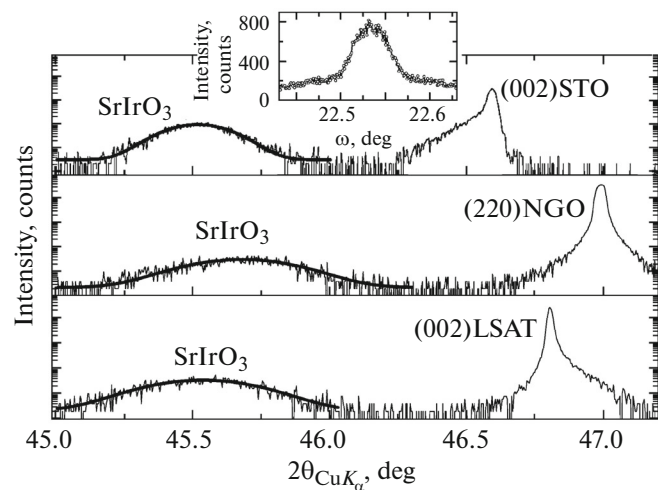
Fig. 2. X-ray diffraction patterns of SrIrO$_3$ films grown on substrates (001) STO, (001) LSAT, and (110) NGO. The inset shows the rocking curve for the film deposited on the STO substrate. The minimum width of the rocking curve at the maximum half-height is 0.05°.
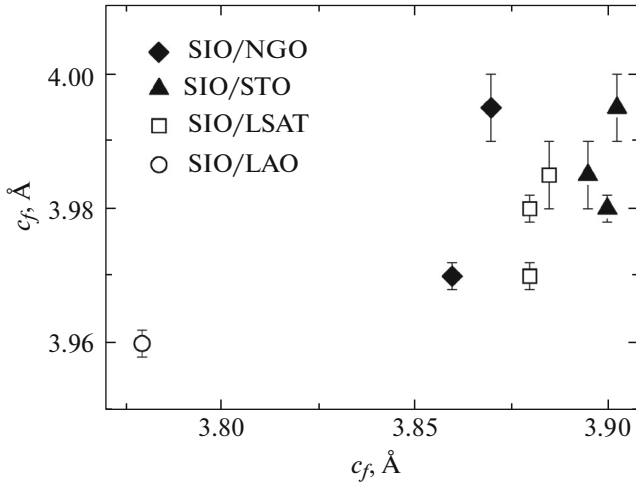
Fig. 3. Dependence of the interplanar distance c_f for SIO films on interplanar placing c_s of substrates LAO, NGO, LSAT, and STO. The measurement error of the interplanar distance of the substrates is less than values of the symbols.
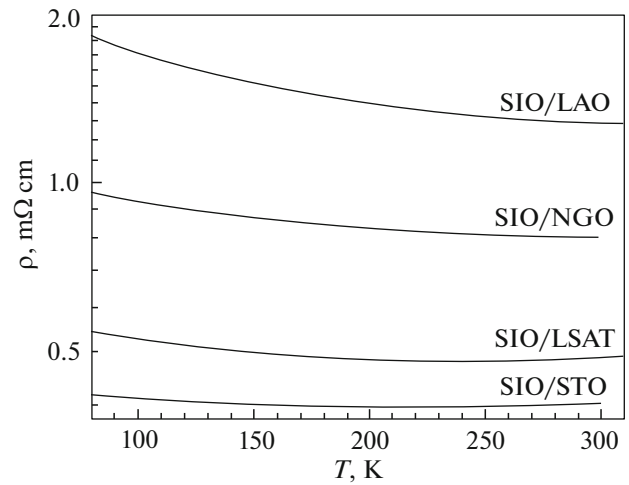
Fig. 4. Temperature dependences of the resistivity of epitaxial SIO films with thickness $d = 90$ nm grown on STO, LSAT, NGO, and LAO substrates.

confirms that the film grows on the substrate by the "cube-on-cube" mechanism.

Figure 2 shows the θ−2θ X-ray diffraction patterns in the vicinity of the second-order reflections from planes perpendicular the substrate plane measured for the SIO films grown on STO, LSAT, and NGO.

The θ−2θ X-ray diffraction patterns (Fig. 2) make it possible to measure the interplanar distances in the film c_f and the substrate in the direction perpendicular to the substrate plane c_s. The dependence of c_f on c_s is shown in Fig. 3. The rocking curve of the film grown on STO has the smallest width (less than 0.05°) (the inset in Fig. 2). It is seen that the interplanar distance of the SIO films is dependent on the size of the substrate unit cell. With increasing the lattice parameters of the pseudocubic substrates from LAO to STO, interplanar distance c_f of the SIO films increases (Fig. 3). The STO substrate has the best mismatch with the metastable perovskite-like phase of SIO.

3. ELECTRON TRANSPORT

Figure 4 shows the temperature dependences of the electrical resistivity of the films deposited on the four substrates. It is seen that the SIO/STO films having the largest lattice parameter c_f exhibit the lowest resistivity. The resistance of the films increases as parameter c_f decreases (Fig. 4). The change in the conductivity of the SIO films with increasing c_s for substrates (001) MgO and (110) GdScO₃ was observed in [10]. Resistivity ρ of the SIO/LAO films at room temperature coincides in order of magnitude with the resistivity of polycrystalline samples obtained at high pressure (2−3 mΩ cm) [14], and the resistivity of the SIO/STO films is an order lower. The resistivity of the SIO/STO

films (about 0.4 mΩ cm) is lower than the limiting value ρ ~3 mΩ cm determined using the Ioffe−Regel−Mott criterion for the metal−insulator transition [19, 20] in the case the lattice parameter of 0.4 nm at the charge carrier concentration of 10^{21} cm⁻³ measured using the Hall effect.

The resistivity of the films increases with decreasing temperature in the case of substrates NGO and LAO, and the SIO/LSAT and SIO/STO films demonstrate a minimum in dependences ρ(T) at temperature T_L. The SIO/STO film demonstrates the minimum in the temperature dependence of the resistivity at $T_L \approx$ 210 K, and this dependence has a metallic character at $T > T_L$. The films deposited on the LSAT substrates have $T_L \approx 250$ K.

It was shown in [17] that SIO films deposited on CdScO₃ substrates with large lattice parameters (in the pseudocubic representation, $c_f = 0.396$ nm) demonstrate a metallic character of the temperature dependence of the resistivity, while similar dependence of SIO/NGO films on the substrates with a smaller parameter $c_f = 0.386$ nm has a dielectric character.

Dependence ρ(T) exhibits a power character in the temperature range, in which the resistivity increases. The temperature dependence of the resistivity of the SrIrO₃ films was described using an approximation [9, 10]

$$\rho = \rho_0 - \alpha T^{3/4} + \beta T^{3/2}, \qquad (1)$$

where ρ_0 is the residual resistivity, α is the parameter of three-dimensional weak localization for systems with strong electron−electron interaction [21]; β is the parameter characterizing an inelastic scattering because of the interaction between electrons and spin subsystem [9, 22]. Figure 5 shows the temperature dependences of the resistivity for the SIO/STO and
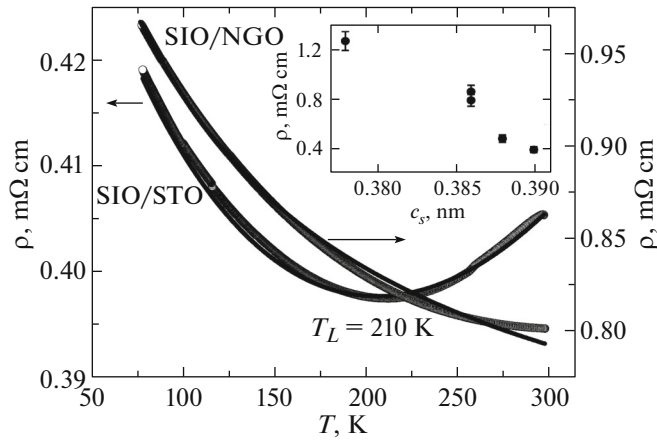
Fig. 5. Temperature dependences of the resistivity of the SIO/STO and SIO/NGO films presented in an enlarged scale. Solid lines are the approximation of the dependences using Eq. (1). The inset shows the dependence of the resistivity of the films at 300 K from tabulated c parameters of the substrates.

Fig. 6. Temperature dependences of the resistivity of epitaxial SIO films with thicknesses 50 and 12 nm grown on the NGO substrate. The inset shows the film conductivity ($d = 12$ nm) in a logarithmic scale as a function of $T^{-1/4}$.

SIO/NGO films and the approximations of these dependences using Eq. (1). The coefficient characterizing a weak localization in the SIO/NGO films $\alpha/\rho = 0.003$ is two times lower than that for the SIO/STO film ($\alpha/\rho_0 = 0.006$). A possible mechanism that determines the localization can be a dislocation shear induced by the film stress; however, the influence of oxygen vacancies should not be excluded as well. Unusual electrical transport properties of SIO can be explained by a distortion of the IrO_6 octahedron that, in turn, leads to the decrease in the orbital overlapping and the formation of a gap in the conduction band. As the mismatch between the film and the substrate increases, the influence of the interaction of electrons with spin subsystem decreases: $\beta/\rho_0 = 5 \times 10^{-5}$ for SIO/STO and $\beta/\rho_0 = 1 \times 10^{-4}$ for SIO/NGO. Similar transition from the metallic character of the temperature dependences of the resistivity to the dielectric character in $BaRuO_3$ with decreasing temperature was noted in [23].

The resistivity of the SIO films on the NGO substrates increases as temperature decreases. The resistivity of the films with thicknesses 50 and 25 nm increases almost twice as temperature varies from 300 to 4.2 K. The resistivity of the film with the smallest thickness $d = 12$ nm increases by a factor of 40, as shown in Fig. 6. According to the model of conduction with variable hopping length [24], at low temperatures, the mean hopping length is larger than the film thickness d, and the conduction is two-dimensional $D = 2$ [24]. In this case, the temperature dependences of the conductivity $\sigma = 1/\rho$ has the form

$$\sigma = \sigma_0 \exp[-(T_0/T)^{1/(D+1)}],$$

where σ_0 and T_0 are the asymptotic parameters found from the experiment. As temperature increases, the

hopping length decreases and becomes less than thickness d, and the temperature dependence of the conductivity in the three-dimensional case $D = 3$ takes the form

$$\sigma = \sigma_0 \exp[-(T_0/T)^{1/4}].$$

Using the approach proposed in [25] for determination of the localization radius a and the density of electronic states at the Fermi level based on the measurements of $R(T)$, we obtain the estimated value $a = 1.8-2.4$ nm for the SIO film with thickness $d = 12$ nm. For this purpose, we found parameters σ_0 and T_0 from experimental dependences $\sigma(T)$ separately for the two- and three-dimensional cases. The two-dimensional character of the hopping conductivity is observed at $T < 8$ K and the three-dimensional character, at $T > 12$ K; the values of T_0 were 1600 ± 10 K and 160 ± 2 K for the cases $D = 3$ and $D = 2$, respectively. Using the obtained value of the localization radius, we can estimate an order of the density of states at the Fermi level $N_F \sim (T_0 a^3)^{-1} = 1.5 \times 10^{22}$ eV^{-1} cm^{-3} that is slightly higher than the theoretical estimation [1].

For the 50-nm-thick SIO/NGO film for which dependence $\rho(T)$ is shown in Fig. 6, the approximation in the $\ln\sigma$ vs. $T^{-1/4}$ coordinates gives value $T_0 \sim 0.1$ K. At such thicknesses, the increase in the film resistance with decreasing temperature can be explained as by a weak localization [21], so a model of disordered metal with the temperature dependence of conductivity $\sigma = \sigma_0 + cT^{1/2}$, where σ_0 and c are experimental constants.

4. CONCLUSIONS

Using laser ablation, we have grown epitaxial films of the $SrIrO_3$ compound with strong spin–orbit interaction on four types of single-crystal substrates. The best quality of the crystal structure (small width of the rocking curve) and the lowest resistivity were obtained for the films deposited on strontium titanate substrate, the lattice parameter of which is nearest to the pseudocubic lattice parameter of the metastable orthorhombic structure of strontium iridate $SrIrO_3$. These films demonstrate the transition of the temperature dependence of conductivity from the metallic to dielectric type at $T = 210$ K. As a whole, the temperature dependences of the film resistivity can be described by the weak localization and the interaction between the electronic and spin subsystems. The weak localization arises due to the appearance of inhomogeneities, which arise, in turn, as a result of dislocation shear in stressed films. As the film thickness decreases to 12 nm, the hopping conduction is observed.

ACKNOWLEDGMENTS

REFERENCES

1. S. Moon, H. Jin, K. Kim, W. Choi, Y. Lee, J. Yu, G. Cao, A. Sumi, H. Funakubo, C. Bernhard, and T. Noh, Phys. Rev. Lett. **101**, 226402 (2008).

2. B. Kim, H. Jin, S. Moon, J. Y. Kim, B. G. Park, C. Leem, J. Yu, T. Noh, C. Kim, S. J. Oh, J. H. Park, V. Durairaj, G. Cao, and E. Rotenberg, Phys. Rev. Lett. **101**, 076402 (2008).

3. A. S. Erickson, S. Misra, G. J. Miller, R. R. Gupta, Z. Schlesinger, W. A. Harrison, J. M. Kim, and I. R. Fisher, Phys. Rev. Lett. **99**, 016404 (2007).

4. J.-M. Carter, V. V. Shankar, M. A. Zeb, and H.-Y. Kee, Phys. Rev. B: Condens. Matter **85**, 115105 (2012).

5. H. Watanabe, T. Shirakawa, and S. Yunoki, Phys. Rev. Lett. **105**, 216410 (2010).

6. A. Shitade, H. Katsura, J. Kunes, X. L. Qi, S. C. Zhang, and N. Nagaosa, Phys. Rev. Lett. **102**, 256403 (2009).

7. X. Wan, A. M. Turner, A. Vishwanath, and S. Y. Savrasov, Phys. Rev. B: Condens. Matter **83**, 205101 (2011).

8. J. M. Longo, J. A. Kafalas, and R. J. Arnott, J. Solidi State Chem. **3**, 174 (1971).

9. F. X. Wu, J. Zhou, L. Y. Zhang, Y. B. Chen, S. T. Zhang, Z. B. Gu, S. H. Yao, and Y. F. Chen, J. Phys.: Condens. Matter **25**, 125604 (2013)

10. J. H. Gruenewald, J. Nichols, J. Terzic, G. Cao, J. W. Brill, and S. S. A. Seo, J. Mater. Res. **29**, 2491 (2014).

11. Y. K. Kim, A. Sumi, K. Takahashi, S. Yokoyama, S. Ito, T. Watanabe, K. Akiyama, S. Kaneko, K. Saito, and H. Funakubo, Jpn. J. Appl. Phys. **45**, L36, (2006).

12. C. Rayan Serrao, J. Liu, J. T. Heron, G. Singh-Bhalla, A. Yadav, S. J. Suresha, R. J. Paull, D. Yi, J. H. Chu, M. Trassin, A. Vishwanath, E. Arenholz, C. Frontera, J. Železný, T. Jungwirth, et al., Phys. Rev. B: Condens. Matter **87**, 085121 (2013).

13. J. Nichols, J. Terzic, E. G. Bittle, O. B. Korneta, L. E. De Long, J. W. Brill, G. Cao, and S. S. A. Seo, Appl. Phys. Lett. **102**, 141908 (2013).

14. J. G. Zhao, L. X. Yang, Y. Yu, F. Y. Li, R. C. Yu, Z. Fang, L. C. Chen, and C. Q. Jina, J. Appl. Phys. **103**, 103706 (2008).

15. G. Cao, V. Durairaj, S. Chikara, L. E. DeLong, S. Parkin, and P. Schlottmann, Phys. Rev. B: Condens. Matter 76, 100402(R) (2007).

16. S. Y. Jang, S. J. Moon, B. C. Jeon, and J. S. Chung, J. Korean Phys. Soc. **56**, 1814 (2010).

17. A. Biswas, K.-S. Kim, and Y. H. Jeong, J. Appl. Phys. **116**, 213704 (2014).

18. L. Zhang, Q. Liang, Y. Xiong, B. Zhang, L. Gao, H. Li, Y. B. Chen, J. Zhou, S.-T. Zhang, Z.-B. Gu, S.-H. Yao, Z. Wang, Y. Lin, and Y.-F. Chen, Phys. Rev. B: Condens. Matter **91**, 035110 (2015).

19. N. E. Hussey, K. Takenaka, and H. Takagi, Philos. Mag. **84**, 2847 (2004).

20. M. Gurvitch, Phys. Rev. B: Condens. Matter **24**, 7404 (1981).

21. P. A. Lee and T. V. Ramakrishnan, Rev. Mod. Phys. **57**, 287 (1985).

22. G. R. Stewart, Rev. Mod. Phys. **73**, 797 (2001).

23. Y. S. Lee, J. S. Lee, K. W. Kim, T. W. Noh, J. Yu, E. J. Choi, G. Cao, and J. E. Crow, Europhys. Lett. **55**, 280 (2001).

24. B. I. Shklovskii and A. L. Efros, *Electronic Properties of Doped Semiconductors* (Springer-Verlag, Berlin, 1984).

25. M. L. Knotek, M. Pollak, and T. M. Donovan, Phys. Rev. Lett. **18**, 853 (1973).

Translated by Yu. Ryzhkov